ACS OMEGA

http://pubs.acs.org/journal/acsodf

Article

Testing the Test: A Comparative Study of Marine Microbial Corrosion under Laboratory and Field Conditions

Camila Canales, Carlos Galarce, Francisca Rubio, Fabiola Pineda, Javiera Anguita, Ramón Barros, Mirtala Parragué, Leslie K. Daille, Javiera Aguirre, Francisco Armijo, Gonzalo E. Pizarro, Magdalena Walczak, Rodrigo De la Iglesia, Sergio A. Navarrete, and Ignacio T. Vargas*

Cite This: *ACS Omega* 2021, 6, 13496−13507

Read Online

ACCESS | Metrics & More | Article Recommendations | Supporting Information

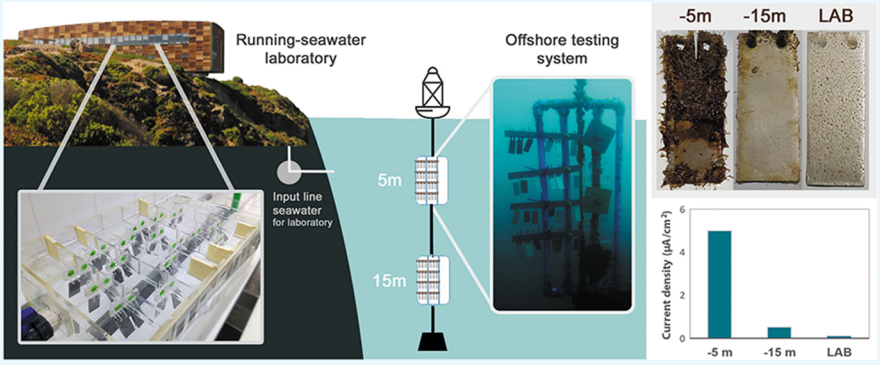

ABSTRACT: Microbially influenced corrosion (MIC) is an aggressive type of corrosion that occurs in aquatic environments and is sparked by the development of a complex biological matrix over a metal surface. In marine environments, MIC is exacerbated by the frequent variability in environmental conditions and the typically high diversity of microbial communities; hence, local and in situ studies are crucial to improve our understanding of biofilm composition, biological interactions among its members, MIC characteristics, and corrosivity. Typically, material performance and anticorrosion strategies are evaluated under controlled laboratory conditions, where natural fluctuations and gradients (e.g., light, temperature, and microbial composition) are not effectively replicated. To determine whether MIC development and material deterioration observed in the laboratory are comparable to those that occur under service conditions (i.e., field conditions), we used two testing setups, in the lab and in the field. Stainless steel (SS) AISI 316L coupons were exposed to southeastern Pacific seawater for 70 days using (i) acrylic tanks in a running seawater laboratory and (ii) an offshore mooring system with experimental frames immersed at two depths (5 and 15 m). Results of electrochemical evaluation, together with those of microbial community analyses and micrographs of formed biofilms, demonstrated that the laboratory setup provides critical information on the early biofilm development process (days), but the information gathered does not predict deterioration or biofouling of SS surfaces exposed to natural conditions in the field. Our results highlight the need to conduct further research efforts to understand how laboratory experiments may better reproduce field conditions where applications are to be deployed, as well as to improve our understanding of the role of eukaryotes and the flux of nutrients and oxygen in marine MIC events.

1. INTRODUCTION

To reproduce environmental conditions in a laboratory is a challenging task, especially when the selected variables to be mimicked correspond to highly dynamic variables in the natural environment where materials are expected to be deployed. Marine and coastal conditions are clear examples of this mismatch and tradeoff between control of experimental conditions and realism. Indeed, marine environments in general and the coastal ocean zone are among the most fluctuating environments due to the complex interaction of winds, bathymetry, coastal topography that modulates hydrographic processes,[1,2] and riverine and other terrestrial inputs, including many human activities.[3] A realistic reproduction of these types of environments represents a major challenge, which is not only due to the number of factors that are involved but also because they are tightly interlinked. The southeastern Pacific coast is an example of a complex and

Received: April 1, 2021
Accepted: April 26, 2021
Published: May 10, 2021

dynamic system subjected to seasonal fluctuations in physicochemical (temperature, salinity, and nutrients) and biological (cellular abundance of phytoplankton) characteristics.[4−8] All of these factors can significantly influence the types of (micro)organisms that colonize living or inert surfaces exposed to seawater and, therefore, the deterioration of metallic structures associated with biofilm development. Thus, understanding the interactions between materials and marine biology (at the micro and macro scales) requires a combination of approaches beyond the controlled laboratory conditions to provide valuable strategies for the preservation and protection of materials and their functionality.[9]

Microbially influenced corrosion (MIC) is a complex phenomenon that involves changes in the chemistry over the metal−liquid interface due to microorganisms' activity, thereby resulting in material degradation and failure.[10] The MIC phenomenon has been investigated via a broad spectrum of experimental strategies. One approach has been the isolation of bacterial groups that have shown a substantial effect on the deterioration of a given material.[11−13] However, this effect is typically identified using culture conditions that do not accurately represent the environment from which these bacteria and other microorganisms were isolated.[14−18] In addition, the effects of environmental conditions (chemical and biological) have been investigated using amended and/or inoculated sterile seawater and controlled temperature, pH, nutrients, and other abiotic conditions. The results of experiments of this type have enabled us to record critical data and collect detailed observations to examine the individual and joint impacts of different variables on the corrosion process and diverse materials when immersed in marine environments.[19−22] However, while such an approach can unveil important biocorrosion mechanisms, it can also result in bias and important shortcomings when results are extrapolated to natural conditions, where the variability of the environmental conditions is the norm and other factors, neglected in the laboratory, might prove to be critical for determining the fate of the biocorrosion process.

Various environmental factors that modify MIC development, such as tides,[23,24] temperature,[25] available nutrients,[26] dissolved oxygen,[25,27] light,[28] and turbulence and currents,[29] cannot be adequately reproduced in the laboratory. The average levels and temporal variability of these factors are highly dependent on the local coastal conditions (e.g., climate and geographical location, among others) and this variation and covariation. These can modulate or completely determine the entire corrosion process of the exposed materials.[30] Several research groups have attempted to mimic these environmental conditions. For instance, Eashwar et al.[28,31,32] built an outdoor system and used it to investigate the effects of sunlight on biofilm development and corrosion. A similar strategy was applied by Fischer et al.[23] and Daille et al.,[24] where the focus was on analyzing the effect of tidal cycles on the biocorrosion of stainless steel (SS). All of these studies have undoubtedly contributed to a better understanding of MIC in marine environments, but there is an urgent need to define the extent to which laboratory experiments that use simulated or natural seawater and conditions can reproduce actual service conditions.

The limitations of representing MIC under laboratory conditions using natural seawater remain unexplored. Therefore, this article compares MIC results between laboratory experiments conducted by pumping fresh-natural seawater pumped from ca. 1.5 m depth to replicated tanks, with experiments conducted in offshore coastal moorings exposed to natural, uncontrolled conditions in the same study area. The methodology consisted of exposing SS 316L coupons at a laboratory scale and comparing their performances with the same type of coupons that were exposed offshore at depths of 5 and 15 m at a marine station at Las Cruces, central Chile. A combination of electrochemical, surface, and biofilm analyses was used to evaluate and compare MIC development. The results demonstrated that a laboratory setup that uses natural seawater could be reliable for investigating the first stages of the formed bacterial biofilm but not for predicting material deterioration or biofouling development in the long term.

2. RESULTS

2.1. Biological Community Composition. Analysis of biological coverage on experimental coupons demanded a separation between micro- and macroorganisms. In terms of macroorganisms, the coupons that were exposed in the laboratory and offshore conditions showed readily observable differences in coverage and number of species. The development of macroalgae was not observed on the coupons that were exposed to laboratory conditions. In contrast, offshore samples that were exposed at both depths were colonized by macroalgae, and variable coverage was observed (Figure 1). At 5 m depth, almost full coverage was observed, and a visual biofouling analysis showed that the most representative species over these coupons were the hydrozoan *Obelia* spp., the encrusting macroalgae *Hildenbrandia lecanellieri*, the large barnacle *Austromegabalanus psittacus*, the tunicate *Pyura*

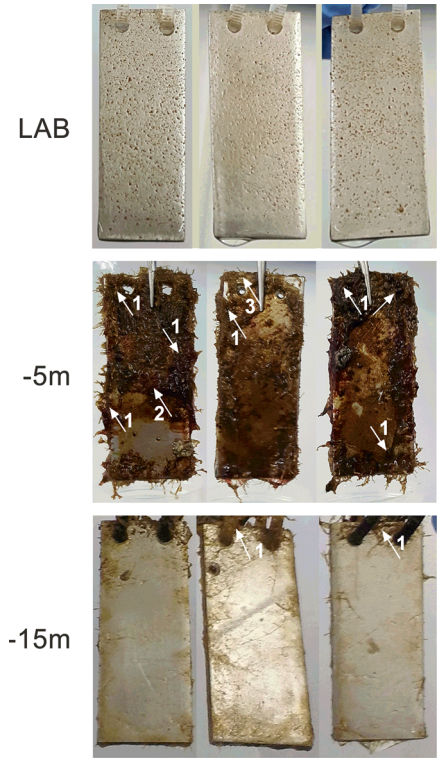

Figure 1. Visual inspection of the biofilms that developed for 70 days under the investigated conditions of immersion exposure (representative coupons). The numbers indicate the representative locations for the following species: (1) *Obelia* spp., (2) *C. rubrum*, and (3) *P. chilensis*.

https://doi.org/10.1021/acsomega.1c01762
ACS Omega 2021, 6, 13496−13507

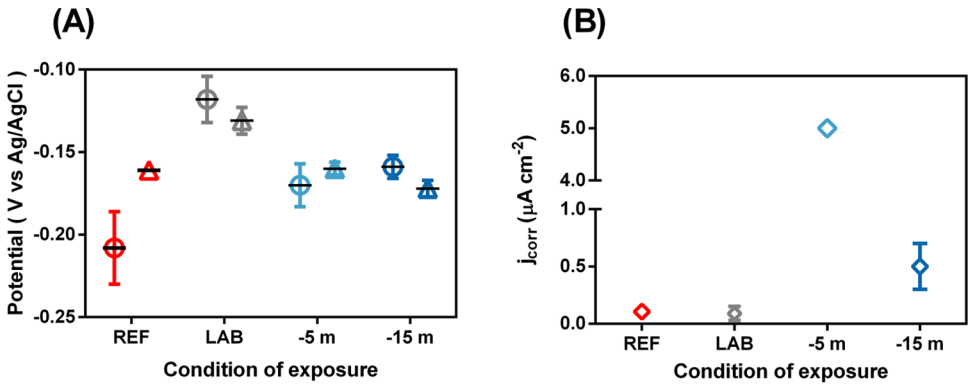

Figure 2. Electrochemical characteristics of SS 316L registered prior to and after exposure under the investigated conditions: (A) values of OCP (circles) and E_{corr} (triangles). The error bars indicate the standard deviation (n = 4). (B) Corrosion currents (diamond) that are determined from the polarization curves. The error bars indicate the standard deviation (n = 2).

chilensis, and the red microalgae *Ceramiun rubrum*. In contrast, the coupons at 15 m depth showed low macrobiological coverage with limited types of macroalgae and dominance by the hydrozoan *Obelia* spp.

A similarity analysis based on restriction fragment length polymorphism (RFLP) profiles of the 16S rRNA gene was carried out to study microorganisms. The similarity analysis revealed a 75% similarity between coupons exposed at 5 m in the field and those in the laboratory setup. In contrast, only 48% similarity was observed between exposure depths 5 and 15 m (Figure S1). These results demonstrate similar microbiological genetic profiles of the core group of bacteria between coupons exposed at 5 m and in the laboratory setup with water pumped from the ocean surface a few hundred meters from the experimental moorings.

2.2. Electrochemical Characterization. *2.2.1. Open-Circuit Potential (OCP) Tendencies and Polarization Curves.* Electrochemical parameters and polarization curves are summarized in Figures 2 and 3, respectively. Additionally, electrochemical parameters that were determined from polarization curves are reported in Table 1. The corrosion potential (E_{corr}) values obtained from polarization curves revealed similar values to the open-circuit potential (OCP) initially measured for each sample (Figure 2A). A shift to anodic values of OCP was observed after 70 days of exposure compared with the reference sample (i.e., clean surface and no previous exposure to the electrolyte), with offset values of 90, 38, and 49 mV after exposure in the laboratory, 5-m-depth, and −15-m-depth setups, respectively (Figure 2A). Furthermore, from the polarization curves, the corrosion currents densities were determined (Figure 2B).

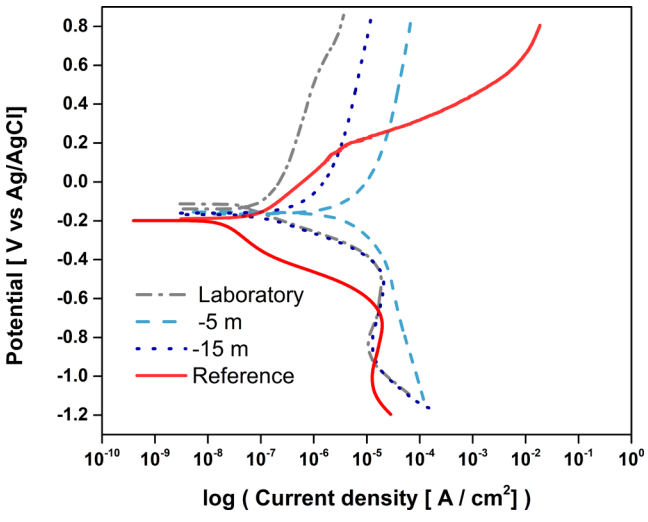

Figure 3. Polarization curves that were registered prior to and after 70 days of exposure under various test conditions. Cathodic and anodic branches are shown together. The values correspond to the average value of two measurements for each branch.

Figure 3 shows the polarization curves obtained for the reference sample and after 70 days of exposure. The cathodic responses that were registered for all coupons were similar in terms of shape and quantity of the current density except for the exposure at a depth of 5 m. The reference coupon shows an anodic response before exposure, which is not passive; hence, pitting instability occurs at potentials above +0.2 V vs Ag/AgCl. After 70 days of exposure, the anodic responses were similar in shape and characteristic of passive responses, although they differed in terms of the quantity of current by one order of magnitude. Unfortunately, the results do not allow suggesting that the surface was passivated because the characteristic plateau was not observed in the anodic curve.

2.2.2. Electrochemical Impedance Spectroscopy (EIS). Figure 4 shows the Nyquist plots and Bode plots obtained for OCP by electrochemical impedance spectroscopy (EIS) before and after 70 days of exposure in each condition. As presented in Figure 4A, the reference coupon (red square) showed the highest charge-transfer resistance (R_{ct}) compared to all coupons after exposure (inset Figure 4A), and all coupons after exposure tended to generate a semicircle shape on the Nyquist plot, especially the coupon that was exposed at 5 m, which presented the lowest R_{ct} (white empty square). This result demonstrates that the coupon that was exposed at 5 m presents charge-transfer processes favored by the deposited biofilm and, for instance, more likely to corrode. The impedance results were comparable to the results that were obtained from the polarization curves. At this depth, the current was two orders of magnitude higher than that of the coupon exposed to laboratory conditions and one order of magnitude higher than that of the coupon exposed at 15 m. Hence, it is expected for the coupon that was exposed at 5 m to present the lowest R_{ct}.

The spectra obtained by EIS for each coupon in the exposure conditions were fitted to different equivalent circuits modeling the processes that occur on the electrode surface,

https://doi.org/10.1021/acsomega.1c01762
ACS Omega 2021, 6, 13496−13507

Table 1. Values of the OCP Registered Prior Polarization and Electrochemical Parameters That Were Determined from the Polarization Curves

condition of exposure	OCP (V)	E_{corr} (V)	current density (μA cm $^{-2}$)	β_c (mV decade^{-1})	β_a (mV decade^{-1})	R_p (kΩ)[b]
REF	−0.208 ± 0.022[a]	−0.161	0.105	113.7	106.3	227.2
LAB	−0.118 ± 0.014	−0.131 ± 0.008	0.09 ± 0.060	129.2 ± 37.3	202.3 ± 20.8	379.8
−5 m	−0.170 ± 0.013	−0.160 ± 0.004	5 ± 0.098	131.2 ± 14.0	254.5 ± 36.7	7.51
−15 m	−0.159 ± 0.007	−0.172 ± 0.005	0.5 ± 0.2	84.4± 7.9	228.6 ± 111.4	53.53

[a]Reference results correspond to the average values of two measurements. E_{corr} was determined using four measurements (two cathodic and two anodic branches). [b]R_p values that are presented were calculated based on the average value for each condition.

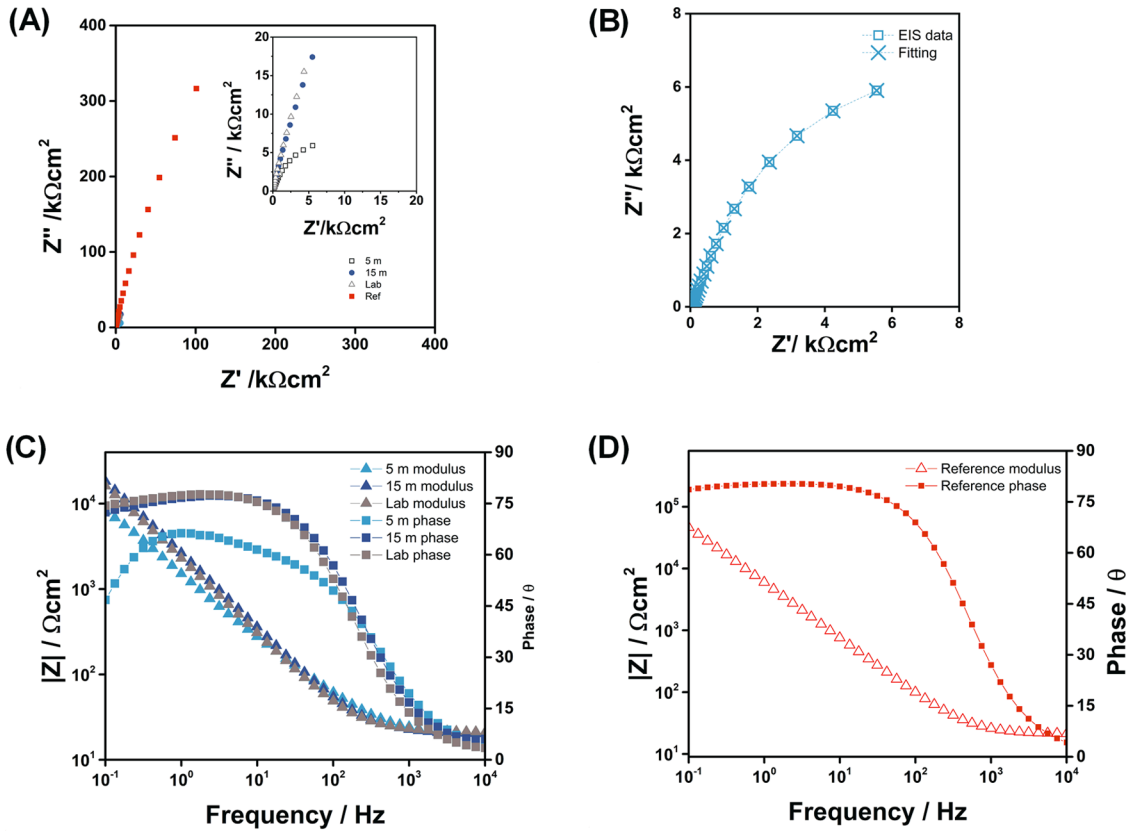

Figure 4. EIS data with the corresponding curve fitting results for SS 316L after exposure to seawater: (A) Nyquist plots for the initial condition and after exposure. The inset shows a detailed view of the low-value scale; (B) curve fitting results for SS 316L after 70 days of exposure 5 m depth, where the empty squares correspond to EIS data and the crosses to the fitted values; (C) Bode phase-angle diagrams (squares) and Bode modulus diagrams (triangles) of samples that were exposed at −5 m (light blue) at −15 m (blue) and under laboratory conditions (gray); and (D) the same data as in (C) for the reference coupon.

Figure 4B shows as an example of the curve fitting result for SS 316L after 70 days of exposure to 5 m depth, where the empty squares correspond to EIS data and the crosses to the fitted values.

Bode plots are shown in Figure 4C,D. According to the phase angles, all coupons after exposure present similar values to the reference coupon (approximately 75°). However, the coupon that was exposed at 5 m, a smaller angle is observed in the intermediate frequency range, which tends to 45° at low frequencies (light blue square); hence, the corrosion processes that occur differ from those of the remaining coupons. Then, the phase-angle value shifts to lower frequencies (approximately 0.1−1 Hz), which corresponds to the presence of a biofilm or the occurrence of depolarization phenomena, produced by the diffusion of different species in the biofilm similar to the phenomenon that was discussed by Domínguez-Benetton et al.[33]

The values of the polarization resistance (R_p) are presented in Table 1. The calculation values were carried out as described in Section 5. The results demonstrated differences among the samples that were exposed to the various test conditions. After 70 days of exposure in the marine environment, the coupons that were exposed at 5 m showed the lowest average value of R_p (7.51 kΩ). This result demonstrated a substantial decrease in the corrosion resistance of SS 316L in this test condition in comparison with the reference value (samples that were immersed in seawater that was filtered at the initial time), which was more than one order of magnitude less than that of the samples that were exposed at 5 m. Figure 5 shows the results obtained from the fitting of the equivalent circuit proposed for the data obtained by EIS (Figure 8 described in Section 5) after 70 days of exposure. From the different bar graphs, it is observed that the dissolution resistance (R_s) maintained a value of approximately 20 $\Omega \cdot cm^{-2}$, which

https://doi.org/10.1021/acsomega.1c01762
ACS Omega 2021, 6, 13496−13507

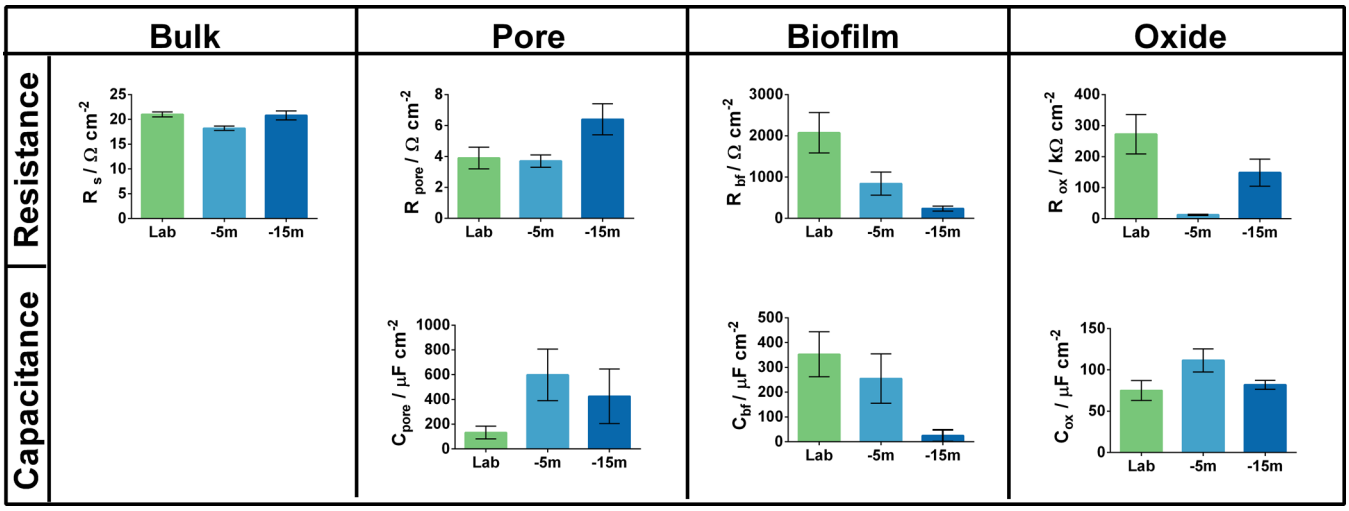

Figure 5. Summary of the electrical quantities that are associated with the proposed ECs. The corresponding values that were determined for the conditions of exposure are displayed in each graph.

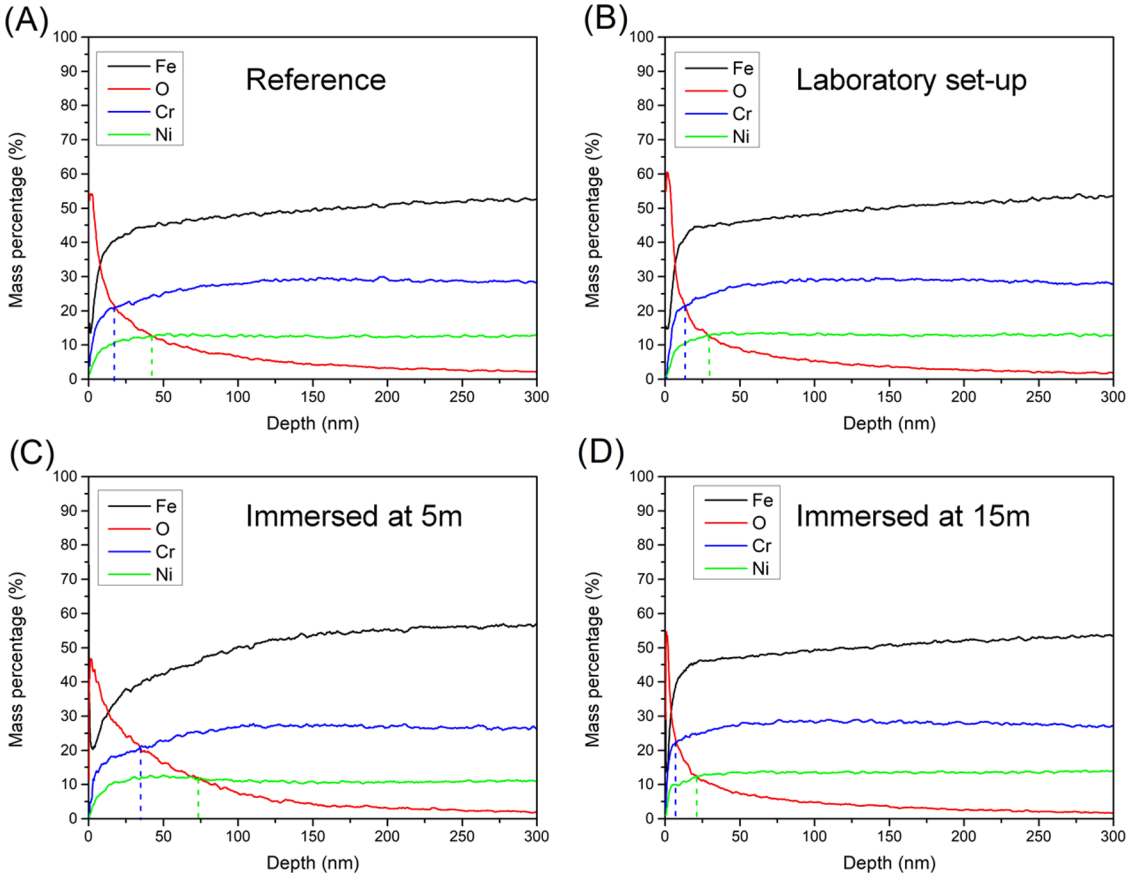

Figure 6. GDOES depth profiles of selected elements that were measured prior and after exposure to seawater: (A) reference (no exposure), (B) laboratory setup, (C) offshore immersion at 5 m, and (D) offshore immersion at 15 m. The vertical dashed lines represent the depths of Cr/O (blue) and Ni/O (green).

matches well with the constant ion concentration of the seawater. Then, regarding the contribution of the biofilms that formed onto the surfaces (aqueous phase + biomass). The pore resistance (R_{pore}), along with the capacitance (C_{pore}), was of the same order of magnitude in all conditions. The similarity in the values was related to the seawater that the biofilm contained within its pores, hence, it was represented as a porous diffuse layer.[34] However, the biofilm resistance (R_{bf}), along with the associated capacitance (C_{bf}), varied when the substrates were immersed at a depth of 15 m. In this case, both parameter values at 15 m depth tend to be less than those for the substrates that were immersed at 5 m and under laboratory conditions. These latter samples present values of the same order of magnitude. Finally, the capacitances of the oxide layer (C_{ox}) present similar values, and the oxide resistance (R_{ox})

https://doi.org/10.1021/acsomega.1c01762
ACS Omega 2021, 6, 13496−13507

values agree with the results obtained from the polarization curves (i.e., R_p).

2.3. Surface Analysis. According to a visual inspection of all samples after 70 days, the corrosion was sufficiently uniform on the surface for the analysis of the chemical composition and thickness of the oxide layer via glow-discharge optical emission spectroscopy (GDOES).

The depth profiles of the chemical composition are shown in Figure 6, in which only the elements that correspond to the metal matrix (Fe), the main alloying elements (Cr and Ni) of the steel, and the main component of the passive layer, namely, oxygen (O), are presented. The native structure of the surface oxide consists of Cr and Ni oxides, and the content of oxygen diminishes exponentially as the depth increases, which is accompanied by a consistent increase in Fe. The 5 m coupons showed a distinctively smoother slope of the oxygen profile than all other samples, which could be associated with a different superficial feature because the higher presence of microorganisms and macroorganisms (Figure 1) increases the surface roughness of this coupon.[35]

In all of the depth plots, the oxygen profile crosses the profiles of the alloying elements. This crossing or intercept was defined in this study as the distance affected by the exposure to seawater and related to the thickness of the oxide layer. Hence, the estimated thickness of the native structure of the oxide layer is approximated to be 42 nm before exposure and 29, 73, and 21 nm after exposure under laboratory conditions and offshore exposure at 5 and 15 m, respectively. These data reveal an inversely proportional relationship between the oxide thickness and the corrosion rate compared with the polarization parameters, namely, the current density and the polarization resistance (R_p), in Table 1. The thickness of the oxide layer determined from the depth profiles is consistent with the values obtained from the Cole−Cole plot (which was obtained from EIS spectra, Figure S2).

3. DISCUSSION

This study was designed to evaluate the differences in the MIC response between the laboratory strategy and direct exposure at sea. Results suggest that the observed biological process (conceptual model) and material performance could be driven by the differences in the environmental conditions encountered in the field. From a biological perspective, the sample that was exposed at 5 m, which is exposed to typically warmer waters above the seasonal thermocline, showed the highest diversity of macroorganisms and the highest biological coverage of the coupons among the tested conditions. The macroalgae species that were identified at both depths are similar to those described in previous reports of macrobiofouling diversity at the same experimental mooring system.[36] The microbiological differences between the laboratory and offshore conditions may be associated with the reductions in the amount and type of organisms ("pool of potential species") that are captured by the pumping system and lifted to the seawater tanks in the laboratory. Coupons exposed to high circulation and flow in the wave-exposed mooring system should, therefore, "sample" a much larger water volume and a larger pool of macro- and microorganism species. Also, conditions for the successful establishment of macroorganisms (e.g., turbulence and water movement) will inevitably vary between lab and mooring conditions. In contrast, since the experiment was conducted during the austral winter months,[36] no differences in temperature or dissolved oxygen were expected at either depth in the water column (Figure S3), and no environmental fluctuations were observed during the exposure time (Figure S4). The differences in coverage that were observed in the coupons that were immersed in the sea can likely be attributed to sunlight conditions. Physicochemical parameters of the seawater measured in the laboratory are described in Table S1.

The activity of phototrophic bacteria and eukaryotes has a crucial role in corrosion processes.[25,37] The presence of macroalgae can create a local increment of dissolved oxygen due to photosynthesis,[22] thereby promoting an increase in the cathodic current and, consequently, increasing the overall corrosion process.[37−39] The presence of photosynthetic organisms was observed clearly in the samples immersed at 5 m, where the complex biomass on the surface influences the observed differences in the current density (Figure 2B) and polarization resistance (Table 1). Nonetheless, given the used experimental design, it was not possible to discriminate and quantify the contribution of microorganisms to these differences over those given by abiotic factors and the presence of macroalgae.

The cluster analysis of RFLP of bacterial biofilms revealed a high similarity between the sample in the laboratory condition and the sample exposed at a depth of 5 m (Figure S1), which were exposed to similar light conditions. This result suggests that after 70 days, a laboratory experiment could represent the early biofilm development on SS surfaces formed in surface seawater. However, these results must be interpreted with caution because few samples for each condition were analyzed, and as mentioned above, it is not possible to separate the biological from abiotic effects. Additionally, the corrosion and biological colonization of coupons that were immersed at sea at 5 m could be underestimated if simulated in a running seawater laboratory. This can be attributed to the presence of an epiphytic community of macroalgae, which was observed in the samples that were exposed in the field. Hence, more and different microorganisms can be incorporated into the biofilm and biofouling compared to the microorganisms under laboratory conditions, which can provide new characteristics to the community.[40−42]

The OCP values obtained in this experiment differ from the values reported by other authors. Nevertheless, these results must be carefully analyzed. In the literature, various OCP values in the MIC response of SS 316L in marine conditions have been reported. For example, L coupons that are exposed to natural seawater present pitting corrosion in a range from +0.5 to +0.6 V (vs Ag/AgCl) after a few days of immersion. Another study that was conducted by Dexter[25] regarded the exposure time and seawater treatment (filtered or nonfiltered) as important factors that can profoundly affect the corrosion potential, and they registered potentials between +0.2 and −0.4 V vs the saturated calomel electrode (SCE). Thus, establishing a potential range can be more suitable when presenting the evolution of the corrosion potential due to the diverse factors that may produce changes in exposed materials, such as the exposure time,[43] the temperature,[44] the chloride concentration[45] and the presence of microorganisms.[22,44,46,47] In this study, the electrochemical reduction process onset around at −0.2 V (vs Ag/AgCl), and a passivation process, that a large amount of biomass might explain, was observed on the coupons. Thus, the formed biofilm and the oxide layer that underlies the biofilm contribute to passivation and may prevent the onset of localized corrosion.

https://doi.org/10.1021/acsomega.1c01762
ACS Omega 2021, 6, 13496−13507

Coupons that are immersed under laboratory conditions are covered by an oxide-biofilm layer that deaccelerates the corrosion processes compared to the other conditions since the corrosion current density was approximately two orders of magnitude lower than that of the coupon that was immersed at a depth of 5 m and one order of magnitude smaller than the coupon that was submerged at a depth of 15 m (Figure 2). The electrochemical response in the coupons exposed to laboratory conditions was similar to the responses described in previous reports.[21,48] The laboratory conditions most likely lack an essential physicochemical parameter and, thus, cannot reproduce the natural marine environment.

Similarly, the electrochemical response of SS 316L supports the significant influence of the micro- and macroorganisms on the surface. Moreover, the reduction of the phase angle at intermediate and low frequencies suggests a decrease in the contribution related to semiconductor-phase formation, which can be due to the corrosion products embedded in a polymeric biofilm/biofouling matrix.[49] This result demonstrates that an adsorption behavior occurred at this depth (5 m), which can be attributed to the adsorption of microorganisms to the metal surface, produced in the layer after 70 days of exposure to diffusion-controlled processes.[49]

The EIS equivalent circuit (EC) used to model MIC revealed the crucial role of the biofilm layer in the system's internal resistance. The differences in the resistances and capacitances can be attributed to the development of a complex biofilm/biofouling matrix on only the sample that was immersed at 5 m, which was composed of macro- and microorganisms unevenly covered the metal surface.

On the other hand, it can be observed that the capacitance values (C_{poro}, $C_{biofilm}$, and C_{ox}) are in the order of μF (Figure 5) similar to studies reported by Ouyang et al.[50] and Yin et al.,[51] which indicates that a microbiological community and ions accumulate on surfaces to form a layer called the packaging film. Along with this, it is also interesting to notice that the values of capacitances and resistances recorded for the biofilm have the following descending order lab > −5 m > −15 m. This indicates the differences in the biofilm and biofouling formed on the surface of 316L SS immersed in seawater. Furthermore, C_{pore} can be considered as the water retention capacity of the biofilm; it is observed that the coupon at a depth of 5 m has the highest capacitance. In addition, it can be observed that numerous biological species are attached to the surface of the metal (Figure 1), which obviously cause changes in its electrochemical behavior.[52] Further, coupons exposed to −15 m present lower C_{bf} and R_{bf} values, which reflects that the formation and the structure of a biofilm influences the processes involved in MIC.[53]

Most likely, macroorganisms (algae) had more influence due to the release of oxygen[22] and the development of a complex biofilm structure.[39] The development of this type of matrix on the exposed surfaces creates a reactive barrier due to the formation of several microgalvanic cells, which can generate fluctuations in the electrochemical responses related to the metal/film interphase. Then, corrosion processes can be promoted.[54] Moreover, the electrochemical response of SS 316L in the samples that were exposed at 5 m could have been influenced not only by abiotic factors and phototrophic organisms but by the production/excretion of enzymes (such as catalase and peroxidase)[55] and other metabolites (such as EPS components), which contribute to metal corrosion.[54,56,57]

No evidence of localized corrosion was obtained via visual inspection of the coupons; thus, the observed changes in the current can be attributed to an increase in the flux of oxygen to the metal surface. According to Bhandari et al.,[58] pit development always initiates due to chemical or physical heterogeneity at the surface, such as inclusions, second-phase particles, solute-segregated grain boundaries, flaws, or plastic deformation by mechanical damage.[58] However, the absence of pitting development in this study suggests a modification by the biofilm/biofouling on the surface. As discussed, this increase could be promoted by phototrophic macro- and microorganisms within the formed biofilm. This effect has been previously reported in experiments that were conducted using specified bacterial strains and culture media conditions.[22,46] Via the same mechanism, the phototrophic activity of the formed biofilm could produce a sufficient supply of oxygen to the reaction sites, which may enhance the formation of oxide at the pitting site and, thus repassivate or heal the damage to the passive film.[58] Therefore, to characterize the process and compare material performance and MIC development between studies, it is crucial to properly consider environmental characteristics and fluctuations and high-resolution characterization of the biological community.

Regarding the GDOES results, the differences that were observed in the depth profiles among the samples that were exposed at 5 and 15 m and under laboratory conditions could explain the variation of the kinetic electrochemical parameters, thereby supporting the presence of a porous structure of oxide layers that is highly superior after exposure at 5 m, which enables the passage of corrosive species toward the metallic bulk. This behavior could be related to the number of macro- and microorganisms on the surfaces that produce a biofilm that might modify the oxides' nucleation and growth process. Indeed, the 5 m coupons, which were the most covered by macro- and microorganisms, showed depth profiles that corresponded to a highly rough surface[35,59] and a possible nonstable oxide layer.[21]

Therefore, the results obtained by both the biological and surface analyses, which included the EIS modeling, suggest a crucial role of the biofilm in the system's electrochemical response and support the importance of designing marine corrosion tests that accurately represent actual environmental conditions.

4. CONCLUSIONS

Based on the results obtained in our study, comparing laboratory experiments with natural field conditions, we conclude that a 70 day laboratory experiment can be useful for investigating microbial biofilm development in SS 316L surfaces that are exposed to surface seawater. The crucial role of the biofilm layer in the system's internal resistance was shown by the EIS EC that was used to model MIC, which is consistent with the early biofouling development and higher corrosion rates that were observed for coupons that were exposed at a depth of 5 m. Finally, the findings of this study have important implications for future MIC studies under marine conditions. Further investigation should be aimed at elucidating eukaryotes' role in the flux of oxygen within the biofilm of MIC events in marine environments.

https://doi.org/10.1021/acsomega.1c01762
ACS Omega 2021, 6, 13496−13507

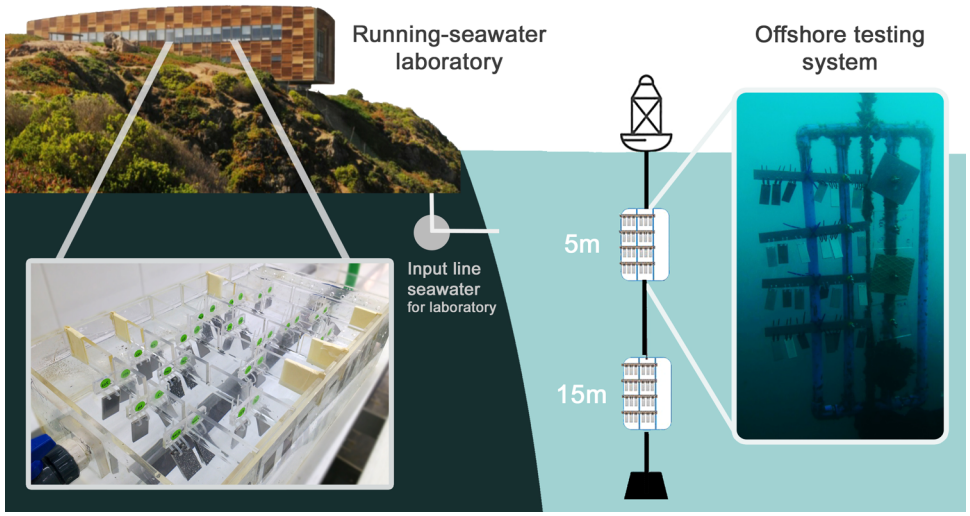

Figure 7. Summary of the experimental setups used for the evaluation of MIC in seawater: A flow-through cell fed by seawater (the laboratory test) and plastic frames that were immersed at the corresponding depth (the offshore test).

5. MATERIALS AND METHODS

5.1. Coupon Preparation. The SS that was used in this study was commercial grade AISI 316L (X2CrNiMo17-12-2, material number 1.4404), which was acquired as a plate with a nominal thickness of 3 mm and 2B surface finish. The chemical composition of the alloy was demonstrated via glow-discharge optical emission spectrometry (Spectruma, GDA 750 HR) bulk analysis to be C 0.006%, Mn 0.94%, Si 0.39%, P 0.37%, S 0.003%, Cr 16.42%, Mo 2.34%, Ni 10.21%, and Fe balance. A total of 18 coupons of 5 × 2 cm^2 were prepared by cutting the plate and drilling two holes to fix the exposure rig. Before exposure, each coupon's surface was ground using emery paper (grit 240), treated with ultrasonication to clean particles' surface, rinsed with distilled water, degreased with ethanol/acetone, and dried by blowing hot air according to ASTM G1-03.[60]

5.2. Experimental Setup. The study was conducted on the coast of the southeastern Pacific Ocean at the Estación Costera de Investigaciones Marinas (ECIM) of the Pontificia Universidad Católica de Chile (PUC), which is located in Las Cruces, central Chile (33°30′16″S; 71°38′23″W). Two testing setups were used to compare SS 316L coupons' responses that were exposed to natural seawater for 70 days. This period was selected based on previous research group experiments, which showed initial bacterial biofilm development.[23] The laboratory conditions consisted of an acrylic tank, where coupons were exposed in a running seawater laboratory (Figure 7), as described by Fischer et al.[23] The offshore testing system consisted of two immersed plastic frames, where samples were submerged at two depths, namely, 5 and 15 m (Figure 7), using the specifications that were reported by Navarrete et al.[36] The exposure was initiated in both setups on the same day, namely, May 21th (fall season), 2017, and was continued through July 31th (winter season), 2017. The variation of the sea temperature was registered during this period, which is presented in Figure S3. The temporal fluctuations of the sea were collected from the satellite data web (Ocean Color Web and ARGANS). A total of six coupons were used for each condition: two for biological analysis and weight loss and four coupons for electrochemical measurements. Coupons from the offshore testing system were sampled by diving at 5 and 15 m depth. After exposure, seawater was used to maintain the recovered coupons in a similar media until analyzed. The used seawater was previously filtered through 10, 3, and 0.2 μm membrane filters (Merck-Millipore), distributed in conical sterile centrifuge tubes and stored until samples were collected.

5.3. Biological Characterization. After exposure, two coupons per condition were used to characterize the biological community. The initial analysis was a nondestructive visual inspection of the coupons, conducted to identify the macroorganisms over the surface. After that, the associated biofilm was analyzed using each coupon. Each coupon was sonicated within the tube's prefiltered seawater with an ultrasonic bath (Jeken PS-20) for 5 min to 40 kHz to recover cells attached to the surface. After sonication, the tube's resultant content was filtered sequentially using 10, 3, and 0.2 μm membrane filters (Merck-Millipore). The membrane filters with the recovered biomass were stored in 2 mL cryovials at −20 °C for DNA extraction. DNA extraction was conducted using a phenol/chloroform protocol.[61]

To broadly analyze variations in the bacterial community within the biofilms, an RFLP profile of 16S rRNA gene amplicons was used. Based on the band pattern on each sample, the absence/presence of a matrix was generated. Hierarchical cluster and nonmetric multidimensional scaling (NMDS) analyses that were based on the Bray−Curtis coefficient were used to visualize the variation in the bacterial community composition using Primer v6.1.7 software.

5.4. Electrochemical Characterization. The OCP, potentiodynamic polarization, and EIS were used to analyze four coupons per condition (5 m, 15 m, and laboratory testing) using a Gamry Ins. (Reference 600 potentiostat/galvanostat/ZRA). Additionally, a reference sample (coupon without exposure) was analyzed to compare its electrochemical behavior. The experimental setup consisted of a one-compartment electrochemical cell with natural seawater as the electrolyte that had been previously filtered to 0.2 μm. All electrochemical studies were completed using SS coupons as working electrodes (WEs) with an exposed area of 1 cm^2, a graphite bar as a counter electrode (CE), and Ag/AgCl (sat. KCl) as a reference electrode (RE). The setup was secured with the clamp system that was provided by the electrochemical cell (PTC1 Paint Test Cell, Gamry Instruments,

https://doi.org/10.1021/acsomega.1c01762
ACS Omega 2021, 6, 13496−13507

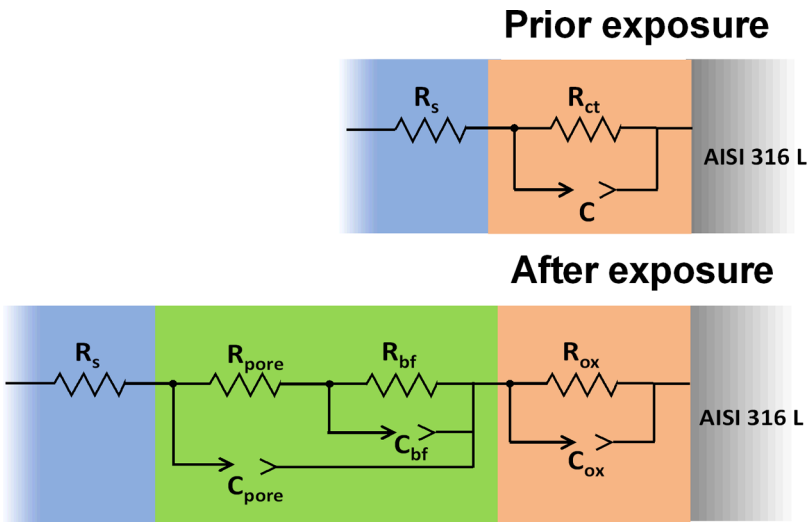

Figure 8. ECs that were used for the curve fitting of the EIS spectra.

Warminster, PA). For each measurement, fresh filtered seawater was used as the electrolyte in the electrochemical cell.

The OCP was measured, until its stabilization, before the electrochemical measurement of coupons. The mean OCP was then calculated for each condition with its respective relative standard deviation (RSD). Subsequently, EIS measurements were conducted for the four coupons within the AC voltage amplitude of ±10 mV per rms vs the mean OCP in the frequency (f) range of 0.01 Hz < f < 100 000 Hz. Finally, potentiodynamic polarization was conducted separately for cathodic and anodic polarization, using a different coupon that was exposed at the same conditions (covered with biofilm) for each experiment. The polarization curves were taken at a scan rate of 0.5 mV·s^{-1} from OCP and presented in a potential window from −1.2 to +0.8 V vs Ag/AgCl. A total of two polarization curves were constructed for each exposure setup (as a result of two anodic and two cathodic curves). For each curve, E_{corr} and the corrosion current (j_{corr}) were determined via an analysis of each branch's Tafel zone separately.

Similarly, R_p was determined using the data obtained from the polarization curves, as described in the ASTM G59.[62] The R_p value was determined after solving eq 1, where β_a and β_c are the Tafel slopes for anodic and cathodic branches of the polarization curve, respectively.

$$B = \frac{\beta_a \beta_c}{2.303(\beta_a + \beta_c)} \quad (1)$$

With the value of the Stern−Geary constant and the corrosion current (j_{corr}), the R_p value was calculated according to eq 2

$$i_{corr} = \frac{B}{R_p} \quad (2)$$

For the EIS analysis, the impedances that were obtained at the OCP were represented as Nyquist and Bode plots. The Nyquist plot illustrates an imaginary component of the impedance ($-Z_{im}$) vs the corresponding real component (Z_{real}), whereas the Bode plot presents both the impedance modulus ($|Z|$) and the phase angle (θ) vs f.[62] The results that were obtained from these studies were analyzed through curve fitting of a proposed EC using Zview software. The ECs that were proposed for curve fitting the EIS data are presented in Figure 8. For the reference sample, free of any biofilm and exposure to any environmental condition, the electrical model consists of a Randles circuit. For modeling the electrical response of the SS that was covered with the biofilm, the EC consisted of an analog circuit that was previously reported by Hang et al.,[63] which included the following electrical elements:

- The electrolyte solution, R_s, which was associated with marine water and its complete matrix.
- The Ohmic resistance in series (R_{pore}) with a subcircuit that was composed of C_{bf} and R_{bf}, which were the parameters that were used to describe the nonideal capacitance of the electrical double layer and the charge-transfer resistance of the biofilm, respectively. R_{pore} contains its corresponding capacitance, namely, C_{pore}. The term "pore" refers to aqueous phases that might be contained in the biomass. Then, the biomass is referred to as BF, which includes micro- and macroorganisms that were deposited onto the oxide layer.
- The Ohmic resistance in series of the oxide layer that was formed over the SS 316L coupons (R_{ox}) with its respective nonideal capacitance, namely, C_{ox}, which was formed immediately over the metal surface and under the biofilm.

Then, to determine the materials' impedance or resistance, the equivalent circuits shown in Figure 8 were fitted using the ZView Software (Scribner Associates). The total impedance of the reference system is decomposed by the charge-transfer resistances of the solution (R_s) and the oxide layer (R_{ox}), where R_{ox} contains a double-layer capacitance. On the other hand, the materials after exposure present the biofilm component as an additional phase over the oxide layer. In this regard, based on Pearson's chi-square test, the model presented in Figure 8 agreed with the experimental results. In this case, the total impedance of the system is decomposed by R_s, R_{bf} (considering porosity in its composition), which enables water content on it (R_{pore}), and R_{ox}. For this model, it is essential to consider that R_{pore} and R_{bf} are in series and included in the same phase over the formation of the oxide layer and, at the same time, exposed to the electrolyte. Finally, all double-layer capacitances (C_{dl}) in parallel with resistors (R_{ct}) were replaced by a capacitance element for more accurate fittings.[64] The quality of fitting to the EC was judged via Pearson's chi-square test according to the resulting value of χ^2.[65] Then, to obtain more precise fitting

https://doi.org/10.1021/acsomega.1c01762
ACS Omega 2021, 6, 13496−13507

results, the capacitance elements, namely, C_{dl}, in the electrical EC were replaced by capacitance elements.[66]

5.5. Physicochemical Surface Analysis. The chemical compositions of the reference sample's oxide layers and clean coupons after exposure to seawater (the same used after biological characterization) were analyzed in-depth via glow-discharge optical emission spectroscopy (GDOES). The analysis was conducted with a Spectruma GDA 750 HR instrument (Spectruma Analytik GmbH) that was equipped with a 2.5-mm-diameter anode and was operated in a DC excitation mode (with a constant voltage of 1000 V and a constant current of 12 mA). The glow was obtained in an argon atmosphere (5.0 quality), and the average discharge pressure was 5×10^{-2} hPa. The sputtering rate was calculated such that the measuring depth was at least 100 μm.

The data's reproducibility was ensured by three analyses on each sample by sputtering three spots on the same surface with random locations, and the results were presented as the average of the three measurements. The quantified profiles of chemical composition vs depth were obtained automatically using standard WinGDOES software.

■ ASSOCIATED CONTENT

Supporting Information

The Supporting Information is available free of charge at https://pubs.acs.org/doi/10.1021/acsomega.1c01762.

Results of cluster analysis of 16S rRNA RFLP data using endonuclease *RsaI* for samples exposed to laboratory and environmental conditions (Figure S1); the Cole−Cole plot obtained from the impedance measurement immerse at 5 m, representing the complex capacitance C as $-C(\mathrm{Im})$ vs $C(\mathrm{Re})$ (Figure S2); data of temperature measured throughout the experiment in depth (Figure S3); data showing the environmental fluctuations in the study area (Figure S4); and the table with the physicochemical parameters of the natural seawater measured in the laboratory (Table S1) (PDF)

■ AUTHOR INFORMATION

Corresponding Author

Ignacio T. Vargas − *Marine Energy Research & Innovation Center (MERIC), Santiago 7520282, Chile; Facultad de Ingeniería, Pontificia Universidad Católica de Chile, Santiago 7820436, Chile;* orcid.org/0000-0001-5974-2795; Email: itvargas@ing.puc.cl

Authors

Camila Canales − *Science Institute & Faculty of Industrial Engineering, Mechanical Engineering and Computer Science, University of Iceland, Reykjavík 107, Iceland*

Carlos Galarce − *Marine Energy Research & Innovation Center (MERIC), Santiago 7520282, Chile; Facultad de Ingeniería, Pontificia Universidad Católica de Chile, Santiago 7820436, Chile*

Francisca Rubio − *Marine Energy Research & Innovation Center (MERIC), Santiago 7520282, Chile; Facultad de Ingeniería, Pontificia Universidad Católica de Chile, Santiago 7820436, Chile*

Fabiola Pineda − *Facultad de Ingeniería, Pontificia Universidad Católica de Chile, Santiago 7820436, Chile; Centro de Nanotecnología Aplicada, Facultad de Ciencias, Universidad Mayor, Santiago 8580745, Chile*

Javiera Anguita − *Marine Energy Research & Innovation Center (MERIC), Santiago 7520282, Chile; Facultad de Ingeniería, Pontificia Universidad Católica de Chile, Santiago 7820436, Chile*

Ramón Barros − *Marine Energy Research & Innovation Center (MERIC), Santiago 7520282, Chile; Facultad de Ciencias Biológicas, Pontificia Universidad Católica de Chile, Santiago 8331150, Chile*

Mirtala Parragué − *Marine Energy Research & Innovation Center (MERIC), Santiago 7520282, Chile; Estación Costera de Investigaciones Marinas, Pontificia Universidad Católica de Chile, El Tabo 2690931, Chile*

Leslie K. Daille − *Marine Energy Research & Innovation Center (MERIC), Santiago 7520282, Chile; Facultad de Ciencias Biológicas, Pontificia Universidad Católica de Chile, Santiago 8331150, Chile*

Javiera Aguirre − *Marine Energy Research & Innovation Center (MERIC), Santiago 7520282, Chile; Escuela de Construcción Civil, Facultad de Ingeniería, Pontificia Universidad Católica de Chile, Santiago 7820436, Chile*

Francisco Armijo − *Marine Energy Research & Innovation Center (MERIC), Santiago 7520282, Chile; Facultad de Química y de Farmacia, Pontificia Universidad Católica de Chile, Santiago 7820436, Chile;* orcid.org/0000-0002-2479-6280

Gonzalo E. Pizarro − *Marine Energy Research & Innovation Center (MERIC), Santiago 7520282, Chile; Facultad de Ingeniería, Pontificia Universidad Católica de Chile, Santiago 7820436, Chile*

Magdalena Walczak − *Marine Energy Research & Innovation Center (MERIC), Santiago 7520282, Chile; Facultad de Ingeniería, Pontificia Universidad Católica de Chile, Santiago 7820436, Chile*

Rodrigo De la Iglesia − *Marine Energy Research & Innovation Center (MERIC), Santiago 7520282, Chile; Facultad de Ciencias Biológicas, Pontificia Universidad Católica de Chile, Santiago 8331150, Chile*

Sergio A. Navarrete − *Marine Energy Research & Innovation Center (MERIC), Santiago 7520282, Chile; Facultad de Ciencias Biológicas, Pontificia Universidad Católica de Chile, Santiago 8331150, Chile; Estación Costera de Investigaciones Marinas, Pontificia Universidad Católica de Chile, El Tabo 2690931, Chile; Center for Applied Ecology and Sustainability (CAPES), Pontificia Universidad Católica de Chile, Santiago 8331150, Chile*

Complete contact information is available at: https://pubs.acs.org/10.1021/acsomega.1c01762

Notes

The authors declare no competing financial interest.

■ ACKNOWLEDGMENTS

This study was supported by the Office Naval Research (Grant NICOP-N62909-17-1-2012). The authors also acknowledge the support that CONICYT provided through FONDEQUIP EQM160091. This study was conducted at the Marine Energy Research & Innovation Center (MERIC) (Project CORFO 14CEI2-28228). In addition, Leslie Daille, Javiera Aguirre, Carlos Galarce, and Javiera Anguita acknowledge Agencia Nacional de Investigación y Desarrollo (ANID) for their doctoral scholarships CONICYT-PCHA/Doctorado Nacional/2014-21140415, 2015-21150171, 2013-21130365, and

2018-21181814, respectively. A special thanks to Mamie Sancy for providing the facilities of her laboratory.

REFERENCES

(1) Lentz, S. J.; Fewings, M. R. The Wind- and Wave-Driven Inner-Shelf Circulation. *Annu. Rev. Mar. Sci.* **2012**, *4*, 317−343.
(2) Largier, J. L. In *Linking Oceanography and Nearshore Ecology: Perspectives and Challenges*, The Oceanography and the Ecology of the Nearshore and Bays in Chile. Proceedings of the International Symposium on Linkages and Dynamics of Coastal Systems: Open Coasts and Embayments, 2002; pp 207−239.
(3) Lalli, C. M.; Parsons, T. R. *Biological Oceanography: An Introduction*; Elsevier, 1997.
(4) Thiel, M.; Macaya, E. C.; Acuña, E.; Arntz, W. E.; Bastias, H.; Brokordt, K.; Camus, P. A.; Castilla, J. C.; Castro, L. R.; Cortés, M.; Dumont, C. P.; Escribano, R.; Fernandez, M.; Gajardo, J. A.; Gaymer, C. F.; Gomez, I.; González, A. E.; González, H. E.; Haye, P. A.; Illanes, J. E.; Iriarte, J. L.; Lancellotti, D. A.; Luna-Jorquera, G.; Luxoro, C.; Manriquez, P. H.; Marín, V.; Muñoz, P.; Navarrete, S. A.; Perez, E.; Poulin, E.; Sellanes, J.; Sepúlveda, H. H.; Stotz, W.; Tala, F.; Thomas, A.; Vargas, C. A.; Vasquez, J. A.; Vega, J. M. A. The Humboldt Current System of Northern and Central Chile - Oceanographic Processes, Ecological Interactions and Socioeconomic Feedback. *Oceanogr. Mar. Biol.* **2007**, *45*, 195−344.
(5) Narváez, D. A.; Poulin, E.; Leiva, G.; Hernández, E.; Castilla, J. C.; Navarrete, S. A. Seasonal and Spatial Variation of Nearshore Hydrographic Conditions in Central Chile. *Cont. Shelf Res.* **2004**, *24*, 279−292.
(6) Tapia, F. J.; Largier, J. L.; Castillo, M.; Wieters, E. A.; Navarrete, S. A. Latitudinal Discontinuity in Thermal Conditions along the Nearshore of Central-Northern Chile. *PLoS One* **2014**, *9*, No. e110841.
(7) Aiken, C. M.; Castillo, M. I.; Navarrete, S. A. A Simulation of the Chilean Coastal Current and Associated Topographic Upwelling near Valparaíso, Chile. *Cont. Shelf Res.* **2008**, *28*, 2371−2381.
(8) Weidberg, N.; Ospina-Alvarez, A.; Bonicelli, J.; Barahona, M.; Aiken, C. M.; Broitman, B. R.; Navarrete, S. A. Spatial Shifts in Productivity of the Coastal Ocean over the Past Two Decades Induced by Migration of the Pacific Anticyclone and Bakun's Effect in the Humboldt Upwelling Ecosystem. *Glob. Planet. Change* **2020**, *193*, No. 103259.
(9) Seyeux, A.; Zanna, S.; Allion, A.; Marcus, P. The Fate of the Protective Oxide Film on Stainless Steel upon Early Stage Growth of a Biofilm. *Corros. Sci.* **2015**, *91*, 352−356.
(10) Vargas, I. T.; Fischer, D. A.; Alsina, M.; Pavissich, J.; Pablo, P.; Pizarro, G. E. Copper Corrosion and Biocorrosion Events in Premise Plumbing. *Materials* **2017**, *10*, No. 1036.
(11) Videla, H. A. Prevention and Control of Biocorrosion. *Int. Biodeterior. Biodegrad.* **2002**, *49*, 259−270.
(12) Videla, H. A.; Herrera, L. K. Microbiologically Influenced Corrosion: Looking to the Future. *Int. Microbiol.* **2005**, *8*, 169−180.
(13) Sheng, X.; Ting, Y.-P.; Pehkonen, S. O. The Influence of Sulphate-Reducing Bacteria Biofilm on the Corrosion of Stainless Steel AISI 316. *Corros. Sci.* **2007**, *49*, 2159−2176.
(14) Bermont-Bouis, D.; Janvier, M.; Grimont, P. A. D.; Dupont, I.; Vallaeys, T. Both Sulfate-Reducing Bacteria and Enterobacteriaceae Take Part in Marine Biocorrosion of Carbon Steel. *J. Appl. Microbiol.* **2007**, *102*, 161−168.
(15) Boudaud, N.; Coton, M.; Coton, E.; Pineau, S.; Travert, J.; Amiel, C. Biodiversity Analysis by Polyphasic Study of Marine Bacteria Associated with Biocorrosion Phenomena. *J. Appl. Microbiol.* **2009**, *109*, 166−179.
(16) Enning, D.; Garrelfs, J. Corrosion of Iron by Sulfate-Reducing Bacteria: New Views of an Old Problem. *Appl. Environ. Microbiol.* **2014**, *80*, 1226−1236.
(17) Yuan, S. J.; Pehkonen, S. O.; Ting, Y. P.; Kang, E. T.; Neoh, K. G. Corrosion Behavior of Type 304 Stainless Steel in a Simulated Seawater-Based Medium in the Presence and Absence of Aerobic Pseudomonas NCIMB 2021 Bacteria. *Ind. Eng. Chem. Res.* **2008**, *47*, 3008−3020.
(18) Wade, S. A.; Javed, M. A.; Palombo, E. A.; McArthur, S. L.; Stoddart, P. R. On the Need for More Realistic Experimental Conditions in Laboratory-Based Microbiologically Influenced Corrosion Testing. *Int. Biodeterior. Biodegrad.* **2017**, *121*, 97−106.
(19) Zhang, H.-J.; Dexter, S. C. Effect of Biofilms on Crevice Corrosion of Stainless Steels in Coastal Seawater. *Corrosion* **1995**, *51*, 56−66.
(20) Dupont, I.; Féron, D.; Novel, G. Effect of Glucose Oxidase Activity on Corrosion Potential of Stainless Steels in Seawater. *Int. Biodeterior. Biodegrad.* **1998**, *41*, 13−18.
(21) Xu, F. L.; Duan, J. Z.; Lin, C. G.; Hou, B. R. Influence of Marine Aerobic Biofilms on Corrosion of 316L Stainless Steel. *J. Iron Steel Res. Int.* **2015**, *22*, 715−720.
(22) Liu, H.; Sharma, M.; Wang, J.; Cheng, Y. F.; Liu, H. Microbiologically Influenced Corrosion of 316L Stainless Steel in the Presence of Chlorella Vulgaris. *Int. Biodeterior. Biodegrad.* **2018**, *129*, 209−216.
(23) Fischer, D. A.; Daille, L.; Aguirre, J.; Galarce, C.; Armijo, F.; Iglesia, R. D.; la Pizarro, G.; Vargas, I.; Walczak, M. Corrosion of Stainless Steel in Simulated Tide of Fresh Natural Seawater of South East Pacific. *Int. J. Electrochem. Sci.* **2016**, *11*, 6873−6885.
(24) Daille, L. K.; Aguirre, J.; Fischer, D.; Galarce, C.; Armijo, F.; Pizarro, G. E.; Walczak, M.; la Iglesia, R.; De; Vargas, I. T. Effect of Tidal Cycles on Bacterial Biofilm Formation and Biocorrosion of Stainless Steel AISI 316L. *J. Mar. Sci. Eng.* **2020**, No. 124.
(25) Dexter, S. C. Role of Microfouling Organisms in Marine Corrosion. *Biofouling* **1993**, *7*, 97−127.
(26) Melchers, R. E. Long-Term Immersion Corrosion of Steels in Seawaters with Elevated Nutrient Concentration. *Corros. Sci.* **2014**, *81*, 110−116.
(27) Melchers, R. E. Microbiological and Abiotic Processes in Modelling Longer-Term Marine Corrosion of Steel. *Bioelectrochemistry* **2014**, *97*, 89−96.
(28) Eashwar, M.; Lakshman Kumar, A.; Sreedhar, G.; Kennedy, J.; Suresh Bapu, R. H. Stainless Steel in Coastal Seawater: Sunlight Counteracts Biologically Enhanced Cathodic Kinetics. *Biofouling* **2014**, *30*, 929−939.
(29) Melchers, R. E. The Effect of Corrosion on the Structural Reliability of Steel Offshore Structures. *Corros. Sci.* **2005**, *47*, 2391−2410.
(30) Traverso, P.; Canepa, E. A Review of Studies on Corrosion of Metals and Alloys in Deep-Sea Environment. *Ocean Eng.* **2014**, *87*, 10−15.
(31) Eashwar, M.; Sreedhar, G.; Lakshman Kumar, A.; Hariharasuthan, R.; Kennedy, J. The Enrichment of Surface Passive Film on Stainless Steel during Biofilm Development in Coastal Seawater. *Biofouling* **2015**, *31*, 511−525.
(32) Eashwar, M.; Subramanian, G.; Palanichamy, S.; Rajagopal, G. The Influence of Sunlight on the Localized Corrosion of UNS S31600 in Natural Seawater. *Biofouling* **2011**, *27*, 837−849.
(33) Domínguez-Benetton, X.; Castaneda, H. In *SRB-Biofilm Growth and Influence in Corrosion Monitoring by Electrochemical Impedance Spectroscopy*, Paper presented at the CORROSION, 2005.
(34) Unsal, T.; Cansever, N.; Ilhan-Sungur, E. Impact of Biofilm in the Maturation Process on the Corrosion Behavior of Galvanized Steel: Long-Term Evaluation by EIS. *World J. Microbiol. Biotechnol.* **2019**, *35*, No. 22.
(35) Thobor, A.; Rousselot, C.; Mikhailov, S. Depth Profiles Study of n(TiN+AlN) Bilayers Systems by GDOES and RBS Techniques. *Surf. Coat. Technol.* **2003**, *174−175*, 351−359.
(36) Navarrete, S. A.; Parragué, M.; Osiadacz, N.; Rojas, F.; Bonicelli, J.; Fernández, M.; Arboleda-Baena, C.; Perez-Matus, A.; Finke, R. Abundance, Composition and Succession of Sessile Subtidal Assemblages in High Wave-Energy Environments of Central Chile: Temporal and Depth Variation. *J. Exp. Mar. Biol. Ecol.* **2019**, *512*, 51−62.

https://doi.org/10.1021/acsomega.1c01762
ACS Omega 2021, 6, 13496−13507

(37) Narenkumar, J.; Alsalhi, M. S.; Arul Prakash, A.; Abilaji, S.; Devanesan, S.; Rajasekar, A.; Alfuraydi, A. A. Impact and Role of Bacterial Communities on Biocorrosion of Metals Used in the Processing Industry. *ACS Omega* **2019**, *4*, 21353−21360.
(38) Baeza, S.; Vejar, N.; Gulppi, M.; Azocar, M.; Melo, F.; Monsalve, A.; Pérez-Donoso, J.; Váquez, C. C.; Pavez, J.; Zagal, J. H.; Zhou, X.; Thompson, G. E.; Páez, M. A. New Evidence on the Role of Catalase in Escherichia Coli Mediated Biocorrosion. *Corros. Sci.* **2013**, *67*, 32−41.
(39) Kalnaowakul, P.; Xu, D.; Rodchanarowan, A. Accelerated Corrosion of 316L Stainless Steel Caused by Shewanella Algae Biofilms. *ACS Appl. Bio Mater.* **2020**, *3*, 2185−2192.
(40) Qian, P.-Y.; Lau, S. C. K.; Dahms, H.-U.; Dobretsov, S.; Harder, T. Marine Biofilms as Mediators of Colonization by Marine Macroorganisms: Implications for Antifouling and Aquaculture. *Mar. Biotechnol.* **2007**, *9*, 399−410.
(41) Lebret, K.; Thabard, M.; Hellio, C. Algae as Marine Fouling Organisms: Adhesion Damage and Prevention. *Adv. Mar. Antifouling Coat. Technol.* **2009**, 80−112.
(42) Compère, C.; Jaffré, P.; Festy, D. Aging of Type 316L Stainless Steel in Seawater: Relationship between Open-Circuit Potential, Exposure Time, and Pitting Potential. *Corrosion* **1996**, *52*, 496−501.
(43) Melchers, R. E.; Jeffrey, R. J. Long-Term Corrosion of Mild Steel in Natural and Uv-Treated Coastal Seawater. *Corrosion* **2014**, *70*, 804−818.
(44) Trigodet, F.; Larché, N.; Morrison, H. G.; Maignien, L.; Thierry, D. Influence of Dissolved Oxygen Content on the Bacteria-Induced Ennoblement of Stainless Steels in Seawater and Its Consequence on the Localized Corrosion Risk. *Mater. Corros.* **2019**, *70*, 2238−2246.
(45) Meguid, E. A. A. E. L.; Mahmoud, N. A.; Gouda, V. K. Pitting Corrosion Behaviour of AISI 316L Steel in Chloride Containing Solutions. *Br. Corros. J.* **1998**, *33*, 42−48.
(46) Javed, M. A.; Neil, W. C.; McAdam, G.; Wade, S. A. Effect of Sulphate-Reducing Bacteria on the Microbiologically Influenced Corrosion of Ten Different Metals Using Constant Test Conditions. *Int. Biodeterior. Biodegrad.* **2017**, *125*, 73−85.
(47) Machuca, L. L.; Bailey, S. I.; Gubner, R. Microbial Corrosion Resistance of Stainless Steels for Marine Energy Installations. *Adv. Mater. Res.* **2012**, *347*−*353*, 3591−3596.
(48) Bin, L.; Ji-zhou, D.; Hou, B. Microbiologically Influenced Corrosion of 316L SS by Marine Biofilms in Seawater. *J. Chinese Soc. Corros. Prot.* **2012**, *32*, 48−53.
(49) Dominguez-Benetton, X.; Castaneda, H. In *SRB-Biofilm Growth and Influence in Corrosion Monitoring by Electrochemical Impedance Spectroscopy*, Paper presented at the CORROSION, NACE-05486, 2005; pp 1−13.
(50) Ouyang, Y.; Zhao, J.; Qiu, R.; Shi, Z.; Hu, S.; Zhang, Y.; Chen, M.; Wang, P. Liquid Infused Surface Based on Hierarchical Dendritic Iron Wire Array: An Exceptional Barrier to Prohibit Biofouling and Biocorrosion. *Prog. Org. Coat.* **2019**, *136*, No. 105216.
(51) Yin, Y.; Cheng, S.; Chen, S.; Tian, J.; Liu, T.; Chang, X. Microbially Influenced Corrosion of 303 Stainless Steel by Marine Bacterium Vibrio Natriegens: (II) Corrosion Mechanism. *Mater. Sci. Eng., C* **2009**, *29*, 756−760.
(52) Brug, G. J.; van den Eeden, A. L. G.; Sluyters-Rehbach, M.; Sluyters, J. H. The Analysis of Electrode Impedances Complicated by the Presence of a Constant Phase Element. *J. Electroanal. Chem. Interfacial Electrochem.* **1984**, *176*, 275−295.
(53) Ziadi, I.; Akrout, H.; Hassairi, H.; El-Bassi, L.; Bousselmi, L. Investigating the Biocorrosion Mechanism of 304L Stainless Steel in Raw and Treated Urban Wastewaters. *Eng. Failure Anal.* **2019**, *101*, 342−356.
(54) Videla, H. A.; Herrera, L. K. Understanding Microbial Inhibition of Corrosion. A Comprehensive Overview. *Int. Biodeterior. Biodegrad.* **2009**, *63*, 896−900.
(55) Landoulsi, J.; El Kirat, K.; Richard, C.; Féron, D.; Pulvin, S. Enzymatic Approach in Microbial-Influenced Corrosion: A Review Based on Stainless Steels in Natural Waters. *Environ. Sci. Technol.* **2008**, *42*, 2233−2242.
(56) Kip, N.; A van Veen, J. The Dual Role of Microbes in Corrosion. *ISME J.* **2015**, *9*, 542−551.
(57) Nguyen, T. M. P.; Sheng, X.; Ting, Y. P.; Pehkonen, S. O. Biocorrosion of AISI 304 Stainless Steel by Desulfo Vibrio Desulfuricans in Seawater. *Ind. Eng. Chem. Res.* **2008**, *47*, 4703−4711.
(58) Bhandari, J.; Khan, F.; Abbassi, R.; Garaniya, V.; Ojeda, R. Modeling of Pitting Corrosion in Marine and Offshore Steel Structures - A Technical Review. *J. Loss Prev. Process Ind.* **2015**, *37*, 39−62.
(59) Yuan, S. J.; Pehkonen, S. O.; Ting, Y. P.; Kang, E. T.; Neoh, K. G. Corrosion Behavior of Type 304 Stainless Steel in a Simulated Seawater-Based Medium in the Presence and Absence of Aerobic Pseudomonas NCIMB 2021 Bacteria. *Ind. Eng. Chem. Res.* **2008**, *47*, 3008−3020.
(60) ASTM G1-03. *Standard Practice for Preparing, Cleaning, and Evaluating Corrosion Test Specimens*, 2017.
(61) Fuhrman, J. A.; Comeau, D. E.; Hagström, A.; Chan, A. M. Extraction from Natural Planktonic Microorganisms of DNA Suitable for Molecular Biological Studies. *Appl. Environ. Microbiol.* **1988**, *54*, 1426−1429.
(62) ASTM International. *ASTM G59-97 (2014) Standard Test Method for Conducting Potentiodynamic Polarization Resistance Measurements*; West Conshohocken, PZ, 2014.
(63) Hang, R.; Ma, S.; Ji, V.; Chu, P. K. Corrosion Behavior of NiTi Alloy in Fetal Bovine Serum. *Electrochim. Acta* **2010**, 5551−5560.
(64) Wang, X.; Mei, J.; Xiao, P. Non-Destructive Evaluation of Thermal Barrier Coatings Using Impedance Spectroscopy. *J. Eur. Ceram. Soc.* **2001**, *21*, 855−859.
(65) Lavos-Valereto, I. C.; Wolynec, S.; Ramires, I.; Guastaldi, A. C.; Costa, I. Electrochemical Impedance Spectroscopy Characterization of Passive Film Formed on Implant Ti−6Al−7Nb Alloy in Hank's Solution. *J. Mater. Sci. Mater. Med.* **2004**, *15*, 55−59.
(66) Cojocaru, A.; Prioteasa, P.; Szatmari, I.; Radu, E.; Udrea, O.; Visan, T. EIS Study on Biocorrosion of Some Steels and Copper in Czapek Dox Medium Containing Aspergillus Niger Fungus. *Rev. Chim.* **2016**, *67*, 1264−1270.

https://doi.org/10.1021/acsomega.1c01762
ACS Omega 2021, 6, 13496−13507